M. Prevosto
IFREMER
29280 Plouzane, France

H. E. Krogstad
SINTEF Industrial Mathematics,
N-7034 Trondheim, Norway

S. F. Barstow
OCEANOR,
Pir-Senteret,
N-7005 Trondheim, Norway

C. Guedes Soares
Instituto Superior Tecnico,
Av. Rovisco Pais,
P-1096 Lisboa, Portugal

Observations of the High-Frequency Range of the Wave Spectrum

This paper takes a new look at the high-frequency range of the wave spectrum. The analysis is based on data sets from two recent field campaigns offshore Portugal and Crete carried out in the MAST II WAVEMOD project, data from the WADIC experiment in the North Sea, and deep-sea data from Haltenbanken and Vøringplatået offshore Norway. In addition, we also show spectra obtained by spectral inversion of ERS-1 SAR imagery. The influence and calibration of wave-measuring instrumentation and the use of wavenumber spectra when comparing spectra from shallow water is emphasized.

1 Introduction

The most striking feature of the frequency spectrum of ocean waves is the occurrence of a high-frequency (HF) tail showing power decays in frequency over various ranges above the main spectral peak. Spectral behavior of this form, also known from stochastic turbulence theory, is usually attributed to some basic physical mechanism and is explained by dimensional and scaling arguments.

In the present paper we briefly review the theory of the high-frequency tail, discuss aspects of its measurement, and present analysis of several data sets from deep to rather shallow water. The analysis confirms a tail generally close to f^{-4}, but with slightly different slopes below and above three times the peak frequency. This is partly explained as an effect of the water depth. For very high sea states, the data suggest a self-similar spectral shape.

2 The High-Frequency Range

The high frequency range of the frequency spectrum of ocean waves shows characteristic power decays with frequency. The *saturation range* consists of frequencies for which the spectral energy has reached its maximum, assumed to be due to wave breaking. An overall maximum saturation level implies a lower bound on the wave period for a given wave height corresponding to a completely saturated spectrum for all frequencies above the peak. The *equilibrium range* concept is adapted from stochastic turbulence theory where it signifies a range where the energy travels between wavenumbers in a stationary fashion.

Phillips (1958) was the first to try to explain the observed behavior of the high-frequency tail. His arguments were based on dimensional analysis, in which he claimed that the saturation range wavenumber spectrum Ψ in deep water is characterized by the water density, ρ, the acceleration due to gravity, g, the wavenumber, k, and its direction θ. As ρ and g are eliminated for dimensional reasons, the expression for Ψ has to be of the form $\Psi(k, \theta) = \alpha k^{-4} D(\theta)$, where α is a constant and the directional distribution D is independent of wavenumber. Making the transformation to the directional spectrum, we obtain the well-known form $S(f) \propto g^2 f^{-5}$ in deep water and $S(f) \propto ghf^{-3}$ in shallow water. Kitaigorodskii has in several publications (e.g., Kitaigorodskii, 1986) refined Phillips's dimensional arguments. Based on a stationary singular solution to Hasselmann's equation, he arrives at $\Psi \propto k^{-3.5}$ above the spectral peak; implying $S(f) \propto f^{-4}$ in deep water. This is an *equilibrium range* where the actual level of the range depends on the energy input. The energy moves through the equilibrium range and is dissipated by wave breaking and turbulence in the saturation range at frequencies about three times above that of the main spectral peak. In an extensive paper, Phillips (1985) revises his original theory and argues that both wave-wave interactions, wind input, and various dissipation mechanisms are active simultaneously in the equilibrium range. In this way, Phillips arrives at the same functional dependence on the wavenumber as the Kitaigorodskii theory; but contrary to Kitaigorodskii, Phillips claims that the equilibrium range extends all the way into the capillary range.

Numerous studies on theory and observations of the high-frequency tail have appeared in the literature, most dealing with rather low seas (Battjes et al., 1987; Resio et al., 1989; Banner, 1990; Hansen et al., 1990). Few studies support Phillips's original f^{-5}-behavior. The observed spectra seem closer to an f^{-4}-tail, but definite support for either the Phillips's modified theory or Kitaigorodskii's theory still seems to be lacking.

When it comes to actually measuring the high-frequency range, a comprehensive review of various techniques has been published by Clayson (1989). The survey examines virtually all contact and remote sensing techniques for observing high-frequency waves both in time and spatial domains. There are several effects that may disturb the measurement of the high-frequency range. Frequently, instrumentation applies electronic anti-aliasing filters which affects the high frequencies. Buoys tend to follow the wave orbital motion instead of measuring at a fixed point, and larger buoys measure an average of the surface elevation over their hull area. Buoys may also have a heave resonance within the HF-range. Apart from instrument effects, the Doppler shift due to a uniform current will affect a fixed instrument measurement. Moreover, identical wavenumber spectra correspond to different frequency spectra in deep and shallow water due to the depth-dependent dispersion relation.

In the present paper, which is basically empirical, we analyze the tail of the spectrum from a variety of instruments. The tail is assumed to be of the form $S(f) = Af^{-n}$ with A and n estimated either by linear regression from the log-transformed spectra,

Contributed by the OMAE Division and presented at the 14th International Symposium and Exhibit on Offshore Mechanics and Arctic Engineering, Copenhagen, Denmark, June 18–20, 1995, of THE AMERICAN SOCIETY OF MECHANICAL ENGINEERS. Manuscript received by the OMAE Division, 1995; revised manuscript received December 6, 1995. Technical Editor: S. K. Chakrabarti.

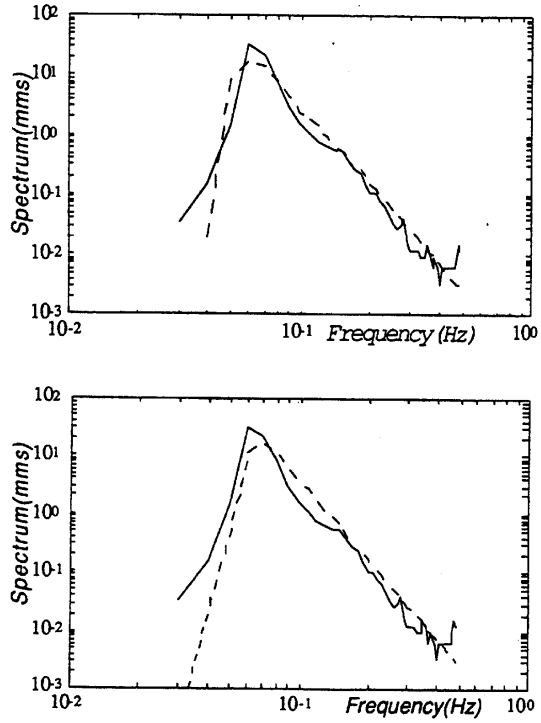

Fig. 1 Deepwater inverted SAR spectra from the December 4, 1993 scene (dashed), Hs = 2.8 m (upper) 3.2 m (lower). Data from a waverider at 72 m water depth about 80 km south of the site shown with a solid line (*Hs* = 3.3 m)

or by a direct maximum likelihood estimation, assuming the appropriate χ^2-distribution for the spectral estimates. The difference between these two approaches is small.

In the following, the significant wave height, *Hs*, and the mean period, *Tz*, are computed from the spectral moments, and *Tp* is the inverse peak frequency *fp*.

3 Analysis of the Data Sets

3.1 Data From the Portuguese Coast. During the MAST-II program WAVEMOD, an area of the exposed west coast of Portugal, just north of the town Figueira da Foz, was instrumented by OCEANOR A/S with three wave buoys in a line perpendicular to the coast (Barstow et al., 1994). Directional waveriders were placed in 20 and 72-m water depths and a nondirectional waverider at 50 m. The Portuguese Hydrographic Institute's directional waverider was also located in the same area in close to 100-m water depth. Measurements in WAVEMOD were carried out from October 1993 to May 1994. The wave climate is swell-dominated as a result of frequent storms further to the north in mid-Atlantic. Significant wave height varied from below 1 m to over 8 m, which occurred during three major storms on January 6 and 10, and February 4; all of which were a result of a combination of high swell and wind sea associated with slow-moving depressions centered close to the British Isles. Currents are relatively weak in this area. For the directional waveriders, directional wave spectra were computed from 1.28 Hz time series for about $\frac{1}{2}$ h each 3 h. Analysis of the buoy data is given in Section 3.3.

During the field experiment, several ERS-1 SAR (original data: © ESA 1994) images were also acquired. The SAR data, showing a clear wave modulation, were subjected to an ocean-SAR spectral inversion algorithm producing directional wave spectra (Krogstad et al., 1994). The corresponding frequency spectra reach up to about 0.21 Hz. Examples of inverted SAR spectra from December 4, 1993, superimposed on buoy spectra are shown in Fig. 1.

Note that the inverted SAR spectra are *extrapolated* by an HF tail with $n = 4.5$ above 0.2 Hz, a decay which is closely matched by the buoy data. Although the SAR can never be expected to be a high-frequency wave recorder, it is nevertheless interesting to observe that the inverted SAR spectra also have a characteristic power decay in frequency *between* the spectral peak and the start of the extrapolation at 0.2 Hz, as shown in Fig. 2. However, since the wave conditions were actually swell-dominated at the time of the recording, the buoy spectra in Fig. 1 indicating a rather sharp peak are probably closer to reality.

The WAVEMOD field campaign was relatively short. However, the Portuguese Hydrographic Institute has carried out wave measurements near the same location since 1981, and these data were also available to the project team.

In order to increase the statistical precision, averaged spectra rather than individual spectra were studied. When determining the average spectra, care was taken in order to guarantee that only similar types of spectra were included. Using the database from 1981 to 1990, all spectra which were identified as having more than one peak were discarded. The criteria adopted to identify multi-peaked spectra are discussed in Guedes Soares and Nolasco (1992). About 28 percent of the spectra were removed for this reason. The fraction is similar to other locations in the North Atlantic (Guedes Soares, 1991). The re-

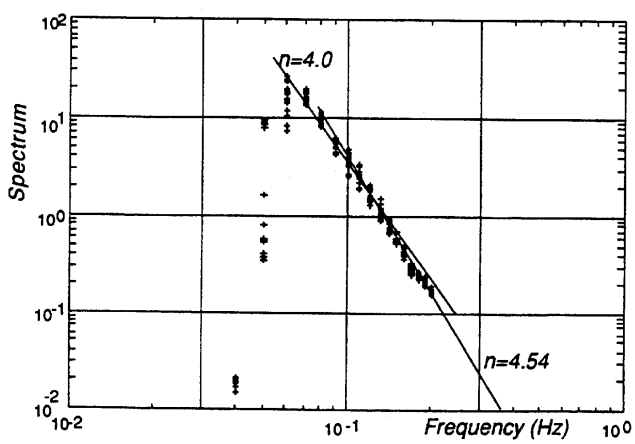

Fig. 2 Thirteen inverted SAR spectra from the outer part of the SAR scene December 4, 1993 illustrating f^{-n} decay

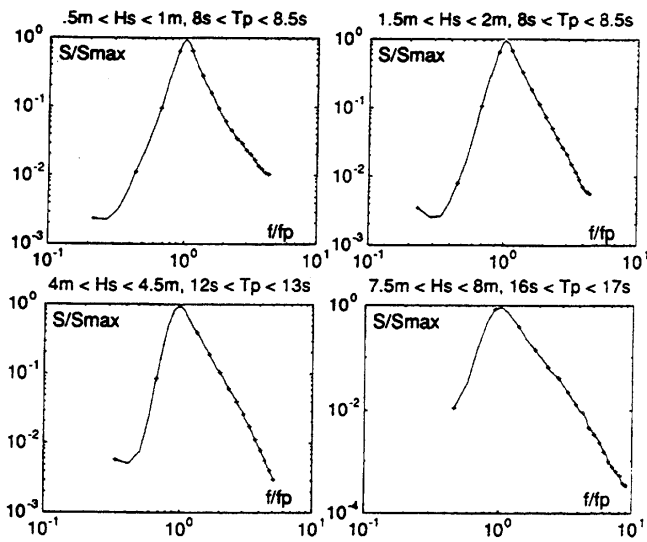

Fig. 3 Examples of averaged spectra from the long-term measurements at Figueira da Foz

Table 1 Exponent of the HF tail obtained by a regression involving all frequencies above the spectral peak (Figueira da Foz long-term data set, 12106 spectra)

Tp(s) Hs(m)	6.5-7	7-7.5	7.5-8	8-8-5	8.5-9	9-9-5	9.5-10	10-11	11-12	12-13	13-14	14-15
0-0.5	3.6	-	4.2	3.6	3.2	3.2	-	2.4	-	-	-	
0.5-1	3.4	3.7	3.2	3.1	3.0	2.9	4.0	3.7	3.1	2.6	2.6	2.5
1-1.5	3.8	3.7	3.7	3.5	3.4	3.3	3.3	3.0	2.9	3.6	3.3	2.9
1.5-2	3.9	3.9	3.8	3.7	3.6	3.5	3.5	3.4	3.2	3.9	4.0	3.6
2-2.5	4.1	4.0	3.9	3.9	3.8	3.7	3.6	3.5	3.4	3.4	3.2	3.8
2.5-3	4.3	4.2	4.1	4.0	3.9	3.8	3.7	3.7	3.6	3.5	3.4	3.3
3-3.5	4.4	4.4	4.3	4.1	4.0	3.9	3.9	3.8	3.8	3.6	3.6	3.5
3.5-4	-	-	4.1	4.3	4.1	4.1	4.0	3.9	3.7	3.7	3.6	3.6
4-4.5	-	-	-	5.0	-	4.1	4.1	4.0	3.9	3.8	3.7	3.7
4.5-5	-	-	-	4.7	4.2	4.2	4.3	4.2	4.0	3.9	3.7	3.7
5-5.5	-	-	-	-	-	4.1	4.3	4.4	4.1	3.9	3.8	3.8
5.5-6	-	-	-	-	-	-	4.3	4.1	3.9	4.1	4.0	3.8
6-6.5	-	-	-	-	-	-	-	-	4.2	4.1	4.0	4.0
6.5-7	-	-	-	-	-	-	-	-	-	-	4.3	4.0
7-7.5	-	-	-	-	-	-	-	-	-	4.4	4.1	4.1
7.5-8	-	-	-	-	-	-	-	-	-	-	-	2.8

maining spectra were then pooled into relatively narrow classes defined by wave height and period (0.5 m for Hs and 0.5 s for Tp). The averaged spectra were formed after being normalized by the maximum value and the peak frequency. This was found to be the most appropriate; but similar results were also obtained by normalizing the spectrum using the total spectral energy instead of the maximum.

Apart from a few cases in which the number of spectra in the class was very small, the average spectra had a very pronounced linear tail in a log-log scale, as shown for a few examples in Fig. 3.

A regression of the logarithm of the average spectra over the whole range above the spectral peak shows exponents ranging from $n = 3$ to 4.5, with a majority between 3.3 and 4.0. However, the tail between fp and $2-3fp$ is less steep than for frequencies above $3fp$. Moreover, for a given wave height, spectra with a short peak period are steeper than spectra with longer periods. The tail also gets more steep when the wave height increases for a given peak period. The variation pattern of the exponent is clearly depicted in Table 1, which shows the exponent of the tail obtained by including all frequencies above the peak frequency. Similar trends were also obtained when the slope of the tail was calculated only for frequencies larger than $2fp$ and $3fp$, although the numerical values were somewhat different (Guedes Soares and Coelho, 1995). In order to express the trends as the one observed in Table 1, a bilinear regression of the form

$$n = \alpha + \beta \cdot Hs[m] + \gamma \cdot Tp[s]$$

has been fitted to the exponents in the *Hs-Tp* table. The final result is given in Table 2.

3.2 Data From Crete. The measurement site was on the northwestern coast of the island of Crete in a small bay, exposed to the north and situated on the western side of the town of Rethymnon. It is exposed to relatively long fetches in the Aegean sea (~200 km) and has a simple topography (slope ~ 2.5 percent) (Barstow et al., 1994). Although summer and winter climatology are quite different, severe sea conditions ($Hs > 4$ m) near shore may occur at any season. Wave directions at the site are predominantly northwest to northeast. Tides are not significant in this area and local currents are essentially wind-

Table 2 Exponents and regression coefficients fitted to the result in Table 1

Regression	α	β	γ	Correlation coefficient	Average n
$fp - 2fp$	4.36	0.015	-0.067	0.51	3.6
$2fp - f_{max}$	4.18	0.324	-0.134	0.73	3.7
$fp - 3fp$	4.02	0.111	-0.070	0.63	3.6
$3fp - f_{max}$	6.62	0.170	-0.255	0.28	4.2
$fp - f_{max}$	4.15	0.186	-0.091	0.81	3.7

Table 3 Results for the high-frequency exponent for $Tp > 8.5$ s and $Hs > 2.5$ m (WAVEMOD data from Crete)

Range:	[1/Tz,3fp]			[3fp,0.6Hz].		
Instrument	Mean	St. dev.	# spec.	Mean	St. dev.	# spec.
Buoy at 100m depth	3.89	0.38	110	4.42	0.36	110
Buoy at 20m depth	3.80	0.37	119	5.24	0.45	118
Buoy at 20m depth [3fp,.55Hz]				4.88	0.52	119
Buoy at 10m depth	3.59	0.31	79	4.71	0.56	95
Fixed point at 100m depth	3.89	0.38	110	3.99	0.32	110
Fixed point at 10m depth	3.40	0.26	77	4.02	0.32	84

generated. The general water circulation amounts to a few centimeters per second.

Three wave buoys were deployed during a 10-mo period along a line approximately perpendicular to the coast. Two directional waveriders were located at 10 and 100 m depth and one nondirectional waverider buoy was located at 20 m depth. In this study, we show results for the subset $Tp > 8.5$ s and $Hs > 2.5$ m consisting of about 100 20-min time series for each buoy sampled at 1.28 Hz (2.56 Hz for the nondirectional buoy).

The power n has been estimated by an ML method for the frequency ranges $[1/Tz, 3fp]$ and $[3fp, 0.6\ \text{Hz}]$. The second frequency range is very short (sometimes equal to zero) for small peak periods. From a simulation study, the sampling variability for n was found to be about 6 percent for the first range and 9 percent for the second.

The waverider applies an *anti-aliasing filter* consisting of a 5th-order Butterworth filter with a cut-off frequency (3 db) at 0.6 Hz. This filter has some effect on the slope near the cut-off frequency (see Table 3).

The measurement of the vertical displacement of the free surface is also modified by the heave transfer function of the buoy which depends on its radius (here 0.7 m for the nondirectional, and 0.9 m for the two others) and the mooring force (Prevosto, 1995). The heave resonance will give a less steep slope in the uppermost frequency band, most pronounced for the 0.9-m radius buoys. This and different moorings may explain the differences we see between the three buoys in the upper frequency band.

The buoys do not follow the elevation of the free surface without horizontal displacement. The magnitude of this displacement depends on the type of the buoy and the stiffness of the mooring. In the instrumentation which has been deployed, the motions of the buoys have been measured to be very close to the orbital motion of the surface particles (Prevosto, 1995), so that the tail of the spectrum can be influenced by such a behavior compared to what is seen by a fixed point probe. Such perturbation has already been observed in Allender et al. (1989) and analyzed by Rademakers (1993). In the present case, we have processed the directional buoy data so as to predict observations from a fixed location. Details are given in Prevosto (1995). The hypothesis is that the buoy follows exactly the vertical displacement of a particle with equilibrium coordinates defining the fixed point and that the orbital motion is elliptical (correct to second order). The results are summarized in Table 3. In deep water, there is no influence in the first frequency band, but a 10-percent decrease of the slope in the high-frequency band. This conclusion agrees with the results of measurement given in Allender et al. (1989, Fig. 10). In shallow water, we observe a slight 6-percent decrease of the slope in the first frequency band and, as in deep water, a more important decrease of 17 percent of the slope in the upper frequency band. From the table, we also notice that the observed sampling variability is of the same order as the results from the simulations, indicating very similar spectra.

In the lowest band, the spectrum is close to f^{-4} in deep water, but reduces to $f^{-3.4}$ at 10 m depth with a correction made for the effect of buoy displacement. In the higher frequency band (above 3 times the peak frequency), the effect of the filter and heave transfer function are difficult to compensate accurately;

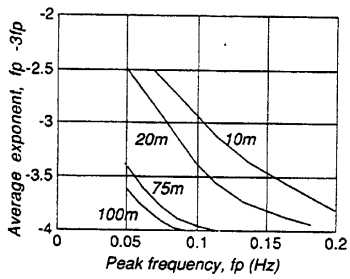

Fig. 4 Average HF-exponent ($-n$) for the range fp–$3fp$ for different water depths assuming $n = 4$ in deep water

but when corrected for the buoy displacement effects, the slope seems much closer to f^{-4} than to f^{-5}, and with no definite depth dependence.

As briefly mentioned in Section 2, due to the depth-dependent dispersion relation, identical wavenumber spectra give rise to different frequency spectra in deep and shallow water by the transformation

$$S(f) = \phi(k)k\frac{dk}{df}, \quad (2\pi f)^2 = gk \tanh(hk)$$

where h is the depth. It is therefore interesting to check whether the results in Table 3 may simply be explained by changes in water depth *assuming* that we have identical wavenumber spectra in deep and shallow water. For a wavenumber spectrum of the Phillips (1985) form, $\phi(k) \propto k^{-3.5}$, the average exponent from fp-$3fp$ has been computed in Fig. 4 for four different water depths. Figure 5 gives the water depth as a function of the highest depth-affected frequency. The data in Table 3 have peak frequencies around 0.10–0.12 Hz. This implies, reading off the graphs, that the 100-m results should not be much affected by the depth, whereas the 10-m measurements should be only slightly affected for $f > 3fp$, but strongly affected in the band fp-$3fp$. For this latter band, Fig. 4 indicates a drop in n from 4 to 3.1; and since the average in Table 3 is not taken from fp, but from the slightly larger $1/Tz$, the observed variation from 4 to 3.4 seems basically to be explained by the difference in water depth.

3.3 North Sea and Norwegian Sea Data. In this section, we present analysis of several offshore data sets from the Norwegian and North Seas. Details about the data acquisition have been given elsewhere (Barstow, 1992; Torsethaugen, 1990). The coastal WAVEMOD data from the directional waveriders at Figueira da Foz (Section 3.1) have been subjected to the same analysis. Table 4 summarizes the data sets. The larger directional buoys WAVESCAN and NORWAVE have diameters about 3 m. The hull-averaging should therefore be more pronounced for these buoys compared to the waveriders. No attempt to compensate for horizontal motion as discussed in Section 3.2 has been carried out.

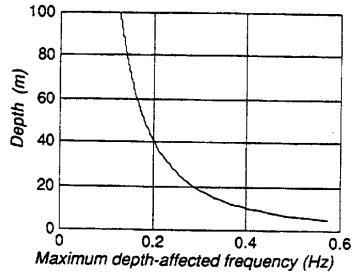

Fig. 5 Approximate maximum spectral frequency affected by the water depth

Table 4 The data set from the North Sea/Norwegian Sea and WAVEMOD

Data set	Depth(m)	Instrument	Period	# spec.
Haltenbanken	~150	NORWAVE/ WAVESCAN	1980-87	12921
Vøringplatået	~1600	WAVESCAN	1987-89	5828
WADIC, reference data set	70	EMI lasers	1985	920
WADIC large buoy	70	WAVESCAN	1985	528
WAVEMOD, Figueira da Foz, 72m	72	Dir. Waverider	1993-94	1389
WAVEMOD, Figueira da Foz, 20m	20	Dir. Waverider	1993-94	1170

The offshore sites have numerous records in excess of 10 m significant wave height. In order to exclude multi-modal spectra from the analysis, the so-called unidirectivity index UI has been applied; see Allender et al. (1989) for a discussion of this parameter. Only spectra having UI > 0.985 have been included. For these data, the frequency range is limited to 0.03–0.47 Hz. The range 3–$5fp$ is thus sometimes truncated by the upper frequency limit.

The data sets range from 20 to 1600 m in water depth. Judging from the conclusion of the previous section, it appears to be reasonable to consider the slope of (nondirectional) wavenumber spectra rather than frequency spectra. The frequency ranges for the fits are similar to the previous analysis. This implies that the relative wavenumber ranges change with water depth and peak frequency. When computing average exponents for various combinations of Hs and Tp, as in Section 3.1, we observe that dimensional analysis that gives the slope exponent n may be written $n = n(s, \ldots)$, where s is the average wave steepness, $s = Hs/\lambda_p$, and where λ_p is the wavelength corresponding to Tp (taking the full dispersion relation into account). Here the dots signify other possible dimensionless combinations of sea state parameters and water depth. On the basis of the observed variations, also evident in Table 1, a simple hypothesis is therefore to assume that n is mainly a function of s. The power n is displayed versus s in Fig. 6. The horizontal line is $n = 3.5$ corresponding to f^{-4} in deep water. In this case, the data were grouped into 1 m × 1 s classes and the average s-parameter and the exponent n were computed for each class with more than five observations. This results in a varying sampling variability, smallest for the large data sets. In most cases, five n increases when s increases. The EMI spectra show an irregular

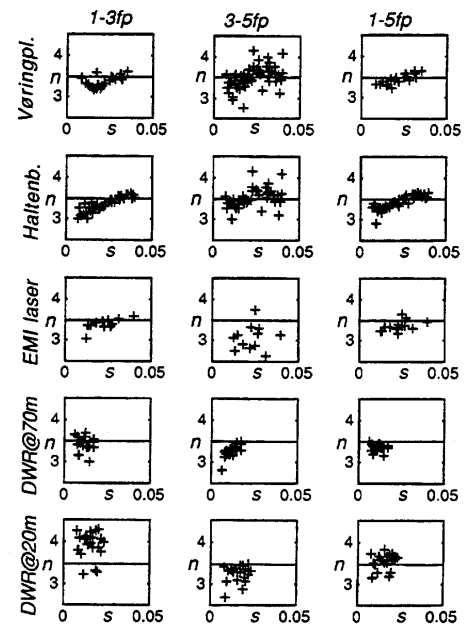

Fig. 6 Average wavenumber spectrum exponent n versus s for the various data sets. The horizontal line corresponds to $n = 3.5$.

Table 5 Average exponents for wavenumber spectra

Data set Hs= 3-6m, Tp = 10-12s	Depth (m)	Wavenumber exponent for the ranges 1-3fp	3-5fp	1-5fp
Vøringplatået	~1600	3.31	3.53	3.48
Haltenbanken	~150	3.35	3.55	3.45
WADIC large buoy	70	3.41	3.30	3.47
WADIC EMI lasers	70	3.39	3.06	3.40
WAVEMOD, Fig. da Foz 1 (Tp =14-16s)	72	3.47	3.36	3.39
WAVEMOD, Fig. da Foz 2 (Tp =14-16s)	20	3.84	3.47	3.59

behavior for the highest range, probably due to noisy data. Data from the two directional waveriders from Figueira da Foz are obviously more swell-dominated than the other sets, and thus cover a smaller s-range. All North Sea/Norwegian Sea data appear to be rather similar. In fact, all sets are similar in the upper band. There is, however, a striking difference between the waveriders in the lowest frequency band, indicating that depth cannot only enter through the dispersion relation.

For a more quantitative analysis, let the dimensionless wavenumber spectrum $\phi_0(x)$ be defined as

$$\phi_0(x) = \phi(xk_p)\frac{16k_p^2}{Hm0}$$

$$(2\pi f_p)^2 = gk_p \tanh(hk_p)$$

where h is the depth and $\phi(k)$ was defined in Section 3.2. Exponents for the tail of the average spectra from a central section of the Tp and Hs joint occurrence table (Hs = 3–6 m, Tp = 10–12 s) are shown in Table 5. (Because of the swell dominance in the data from Portugal, the data selection was moved to somewhat longer periods.) Apart from laser data from WADIC, which are noisy for high frequencies, the behavior is strikingly close to $n = 3.5$ in all cases. The waveriders from Figueira da Foz and the WAVESCAN buoy from WADIC show spectra that are slightly steeper in the first range, whereas the opposite is true for the deep-water buoy measurements. This difference is well illustrated for average spectra from Vøringplatået (depth ~1600 m) and the inner Figueira da Foz directional waverider (depth 20 m) in Fig. 7.

Although we do not find a complete depth-independent behavior for the wavenumber spectra, it is nevertheless obvious that the differences in the slope are much smaller for wavenumber spectra than for frequency spectra. It therefore appears to be reasonable to use wavenumber spectra instead of frequency spectra when comparing data from several water depths in order to eliminate the effect of the depth-dependent dispersion relation.

Returning to the more familiar frequency spectrum, the North Sea/Norwegian Sea data contain several records with very high significant wave height. Exponents for the HF-tail of the frequency spectrum for data with $Hs > 9$ m are given in Table 6. The exponents show a similar behavior to the previous analyses, but the WAVESCAN buoy in the WADIC experiment indicates a somewhat steeper tail. This is probably partly due to the effect of the hull-averaging and may also be due to the horizontal motion, as discussed in Section 3.2.

Table 6 Exponents of the high-frequency tail for very high sea states

Data set	1-3fp	3-5fp	1-5fp	# spec.
Haltenbanken, Hs > 9 m	3.92	4.38	4.09	42
Vøringplatået, Hs > 9 m	3.85	4.32	4.01	25
WADIC, EMI laser, Hs > 9 m	4.01	4.43	4.04	10
WAVESCAN, WADIC Hs > 9m	4.24	4.60	4.29	4

As the wave height increases, the occurrence of multi-modal spectra decreases and the wave spectra tend to become similar in shape. If we use Hs and fp as our characterizing parameters, we may thus assume that the spectrum $S(f)$ can be expressed in terms of a dimensionless spectrum $S_0(x)$ with integral 1 as

$$S(f) = \frac{Hs^2}{16fp} S_0(f/fp)$$

A scatter plot showing all dimensionless spectra with $Hs > 9$ m from Haltenbanken is given in Fig. 8. To the right is shown the observed variability in the spectral values as a function of frequency compared to the *intrinsic* spectral variability $(2/\nu)^{1/2}$, where ν is the degrees of freedom in the spectral estimate (16 in the present case). The observed variability above the spectral peak is only slightly larger than this lower bound. Below the spectral peak, the spectra are strongly varying and the variability is larger. See also Guedes Soares (1990) for similar observations. This clearly suggests a self-similar spectral form.

Dimensionless average spectra from Haltenbanken and the EMI lasers and the WAVESCAN buoy from WADIC are given in Fig. 9. The average EMI spectrum is compared to the average buoy spectrum from Haltenbanken to the left and to the WAVESCAN spectrum from WADIC to the right. The similarities are striking, even if the Haltenbanken and Ekofisk areas have quite different wave climates. It is easy to fit simple power functions to the average spectra. Since the integral of the dimensionless spectrum is 1, such spectra are defined only by the exponents in the various ranges and a requirement of continuity; e.g., a simple fit to the plot in Fig. 9 gave the expression

$$S_0(x) = \begin{cases} 2.3x^9, & x < 1 \\ 2.3x^{-3.9}, & 1 < x < 3, \\ 3.609x^{-4.31}, & 3 < x \end{cases}$$

Obviously, other parametrizations based, e.g., on the JONSWAP form could equally well have been used.

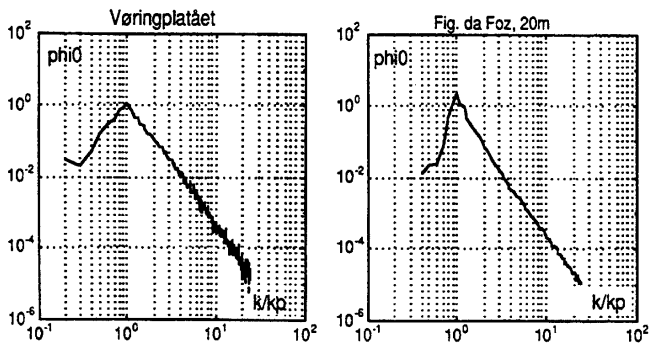

Fig. 7 Average nondimensional wavenumber spectra from Vøringplatået (1600 m) and Figueira da Foz (20 m) illustrating slightly different spectral behavior

4 Conclusions

In the present paper, we have discussed and analyzed data on the high-frequency tail of the wave spectrum from a variety of data sources. All data suggest a power decay near f^{-4} in deep water and none of the data support the original Phillips theory of an f^{-5}-high-frequency tail.

When measuring the high-frequency tail, care should be exercized in order to avoid interpreting instrument deficiencies such as finite extension averaging and horizontal motion of the buoys as features of the tail. Most of the data in the present study indicate that the frequency spectrum is somewhat steeper above $3fp$ as compared to the range between fp and $3fp$; but the differences may in many cases basically be explained by assuming a depth invariant wavenumber spectrum and applying the depth-dependent dispersion relation. When comparing data from various water depths, it is therefore preferable to use wavenumber spectra instead of frequency spectra.

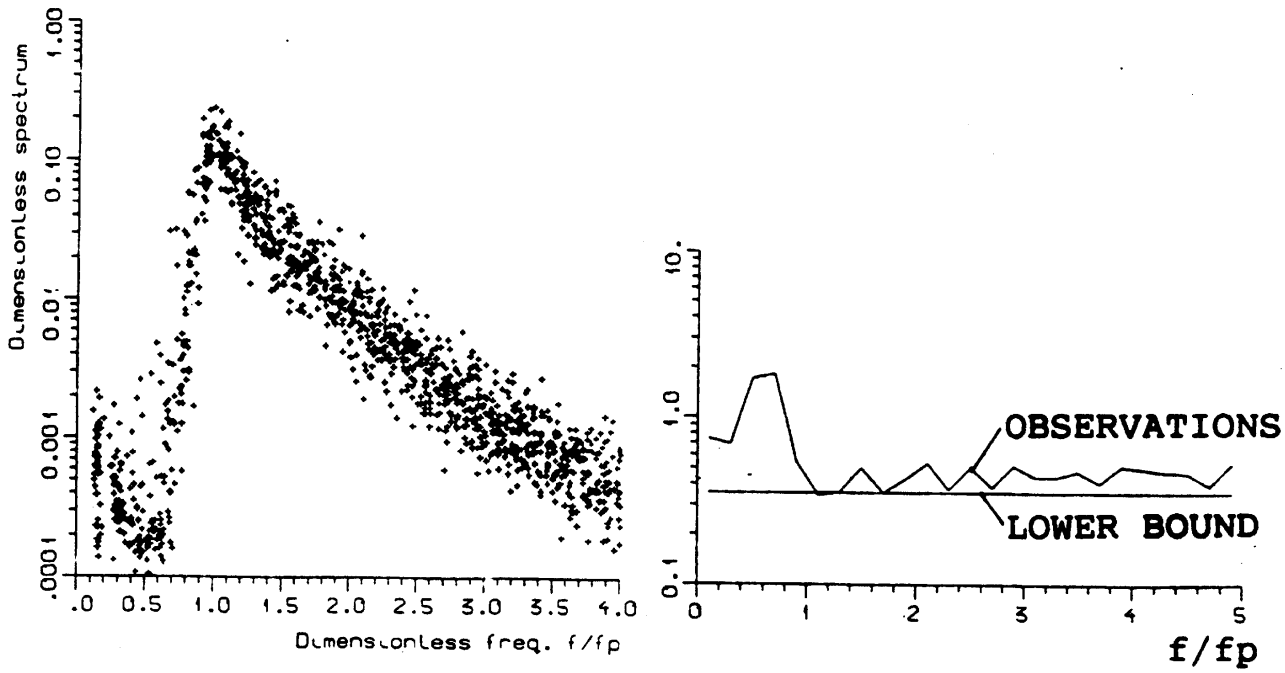

Fig. 8 Dimensionless spectra from Haltenbanken for *Hs* > 9 m shown to the left and the sampling variability to the right

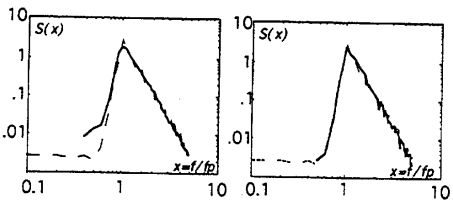

Fig. 9 Average dimensionless spectra for *Hs* > 9 m. Buoy spectra from Haltenbanken (solid) and EMI-laser (dashed) to the left. Wavescan from WADIC (solid) and EMI laser (dashed) to the right.

The exponents for the tails of the wavenumber spectra show less variation in the exponents than the frequency spectra, and a simple model spectrum with a tail $\propto k^{-3.5}$ may be applicable both in deep and shallow water.

The steepness of the tail of average spectra vary for different combinations of *Hs* and *Tp*. In general, one finds steeper tails for steeper sea states where the wave steepness is defined $s = Hs/\lambda_p$.

The deep-water high sea state spectra in the present study have a definite self-similar form. This suggests, at least in deeper water, that one single spectral form could be used for high sea states.

Acknowledgments

This work has been carried out in the MAST II WAVEMOD project, in part funded by the Commission of the European Communities, contract no. MAS2-CT92-0025.

The long-term data from Figueira da Foz were supplied by the Portuguese Hydrographic Institute for the project *Wave Climate and Ship Behaviour in the Portuguese Exclusive Economic Zone,* financed by the Portuguese Research Agency (JNICT) under contract No. PMCT/MAR/931/90 with IST.

Data from the WADIC project were provided by OCEANOR, as were the data from Haltenbanken, which were collected in the ODAP project, and from Vøringplatået, collected by OCEANOR for the Norwegian Petroleum Directorate.

References

Allender, J., Audunson, T., Barstow, S. F., Bjerken, S., Krogstad, H. E., Steinbakke, P., Vartdal, L., Borgman, L. E., and Graham, C., 1989, "The WADIC Project: A Comprehensive Field Evaluation of Directional Wave Instrumentation," *Ocean Engineering,* Vol. 16, pp. 505–536.

Banner, M. L., Jones, I. S. F., and Trinder, J. C., 1989, "Wavenumber Spectra of Short Gravity Waves," *Journal of Fluid Mechanics,* Vol. 198, pp. 321–344.

Barstow, S. F., 1992, "Environmental Conditions in the Norwegian Sea at Vøringplatået (in Norwegian)," OCEANOR report no. R92005.

Barstow, S. F., Paillard, M., and Guedes Soares, C., 1994, "Field Measurements of Coastal Waves and Currents in the WAVEMOD Project," *Proceedings, OCEANS 94 OSATES Conference,* Brest, France, September Vol. I, pp. 487–492.

Battjes, J. A., Zitman, T. J., and Holthuisen, L. H., 1987, "A Re-Analysis of the Spectra Observed in JONSWAP," *Journal of Physical Oceanography,* Vol. 17, No. 8, pp. 1288–1295.

Clayson, C. H., 1989, "Survey of Instrumentation Methods for the Determination of the High Frequency Wave Spectrum," Reports of Institute of Oceanographic Science, Deacon Lab. No. 267.

Guedes Soares, C., 1990, "Effect on Spectral Shape Uncertainty in the Short Term Wave-Induced Ship Responses," *Applied Ocean Research,* Vol. 12, pp. 54–69.

Guedes Soares, C., 1991, "On the Occurrence of Double Peaked Wave Spectra," *Ocean Engineering,* Vol. 8, pp. 167–171.

Guedes Soares, C., and Nolasco, M. C., 1992, "Spectral Modeling of Sea States With Multiple Wave Systems," ASME JOURNAL OF OFFSHORE MECHANICS AND ARCTIC ENGINEERING, Vol. 114, pp. 278–284.

Guedes Soares, C., 1993, "Probabilistic Methodology for Coastal Site Investigation Based on Stochastic Modelling of Waves and Currents," presented at *MAST Days,* Brussels, Belgium, March 15, 16.

Guedes Soares, C., Krogstad, H. E., and Prevosto, M., 1994, "WAVEMOD Project: Probabilistic Models for Coastal Site Investigations," *Proceedings, OCEANS 94 OSATES Conference,* Brest, France, Sept. Vol. I, pp. 493–497.

Guedes Soares, C., and Coelho, J. E., 1995, "Analysis of the High-Frequency Range in Spectra of Figueira da Foz," Report TEC-2.1-03(0), WAVEMOD project.

Hansen, C., Katsaros, K. B., Kitaigorodskii, S. A., and Larsen, S. E., 1990, "The Dissipation Range of Wind-Wave Spectra Observed on a Lake," *Journal of Physical Oceanography,* Vol. 20, No. 9, pp. 1264–1277.

Kitaigorodskii, S. A., 1986, "The Equilibrium Ranges in Wind-Wave Spectra: Physical Arguments and Experimental Evidence for and Against Their Existence," *Wave Dynamics and Radio Probing of the Ocean Surface,* eds., O. M. Phillips and K. Hasselmann, Plenum Press, New York, NY, pp. 9–40.

Krogstad, H. E., Samset, O., and Vachon, P. W., 1994, "Generalizations of the Nonlinear Ocean-SAR Transformation and a Simplified SAR Inversion Algorithm," *Atmosphere and Ocean,* Vol. 32, pp. 61–82.

Phillips, O. M., 1958, "The Equilibrium Range in the Spectrum of Wind-Generated Waves," *Journal of Fluid Mechanics,* Vol. 4, pp. 426–434.

Phillips, O. M., 1985, "Spectral and Statistical Properties of the Equilibrium Range in Wind-Generated Gravity Waves," *Journal of Fluid Mechanics,* Vol. 156, pp. 505–531.

Prevosto, M., 1995, "Influence of Buoy Behaviour on Measured Wave Characteristic," Report TEC-2.3-02(0), WAVEMOD project.

Prevosto, M., 1995, "The High Frequency Tail of the Wave Spectrum—Greek Site Database Analysis," Report TEC-2.1-06(0), WAVEMOD project.

Rademakers, P. J., 1993, "Technical Note: Waverider-Wavestaff Comparison," *Ocean Engineering,* Vol. 20, No. 2, pp. 187–193.

Resio, D., and Perrie, W., 1989, "Implications of an f^{-4} Equilibrium Range for Wind-Generated Waves," *Journal of Physical Oceanography,* Vol. 19(2), pp. 193–204.

Torsethaugen, K., 1990, "Haltenbanken Area Metocean Study, Norwegian Hydrotechnical Laboratory," Report STF60 A90053.